

Washington University School of Medicine

Digital Commons@Becker

Open Access Publications

2019

Regional differences in the expression of tetrodotoxin-sensitive inward Ca^{2+} and outward Cs^{+} / K^{+} currents in mouse and human ventricles

Wei Wang

Rebecca L. Mellor

Jeanne M. Nerbonne

C. William Blake

Follow this and additional works at: https://digitalcommons.wustl.edu/open_access_pubs



Regional differences in the expression of tetrodotoxin-sensitive inward Ca^{2+} and outward Cs^+/K^+ currents in mouse and human ventricles

Wei Wang, Rebecca L. Mellor, Jeanne M. Nerbonne & C. William Balke

To cite this article: Wei Wang, Rebecca L. Mellor, Jeanne M. Nerbonne & C. William Balke (2019) Regional differences in the expression of tetrodotoxin-sensitive inward Ca^{2+} and outward Cs^+/K^+ currents in mouse and human ventricles, *Channels*, 13:1, 72-87, DOI: [10.1080/19336950.2019.1568146](https://doi.org/10.1080/19336950.2019.1568146)

To link to this article: <https://doi.org/10.1080/19336950.2019.1568146>



© 2019 The Author(s). Published by Informa UK Limited, trading as Taylor & Francis Group.



[View supplementary material](#)



Published online: 01 Feb 2019.



[Submit your article to this journal](#)



Article views: 684



[View related articles](#)



[View Crossmark data](#)

RESEARCH PAPER



Regional differences in the expression of tetrodotoxin-sensitive inward Ca^{2+} and outward Cs^+/K^+ currents in mouse and human ventricles

Wei Wang^a, Rebecca L. Mellor^a, Jeanne M. Nerbonne^{a,b}, and C. William Balke^{a,b}

^aCenter for Cardiovascular Research, Department of Medicine, Cardiovascular Division, Washington University School of Medicine, St. Louis, MO, USA; ^bJohn Cochran Veterans Administration Medical Center, St. Louis, MO, USA

ABSTRACT

Tetrodotoxin (TTX) sensitive inward Ca^{2+} currents, $I_{\text{Ca}(\text{TTX})}$, have been identified in cardiac myocytes from several species, although it is unclear if $I_{\text{Ca}(\text{TTX})}$ is expressed in all cardiac cell types, and if $I_{\text{Ca}(\text{TTX})}$ reflects Ca^{2+} entry through the main, Nav1.5-encoded, cardiac Na^+ (Nav) channels. To address these questions, recordings were obtained with 2 mM Ca^{2+} and 0 mM Na^+ in the bath and 120 mM Cs^+ in the pipettes from myocytes isolated from adult mouse interventricular septum (IVS), left ventricular (LV) endocardium, apex, and epicardium and from human LV endocardium and epicardium. On membrane depolarizations from a holding potential of -100 mV, $I_{\text{Ca}(\text{TTX})}$ was identified in mouse IVS and LV endocardial myocytes and in human LV endocardial myocytes, whereas only TTX-sensitive outward Cs^+/K^+ currents were observed in mouse LV apex and epicardial myocytes and human LV epicardial myocytes. The inward Ca^{2+} , but not the outward Cs^+/K^+ , currents were blocked by mM concentrations of MTSEA, a selective blocker of cardiac Nav1.5-encoded Na^+ channels. In addition, in Nav1.5-expressing tsA-201 cells, $I_{\text{Ca}(\text{TTX})}$ was observed in 3 (of 20) cells, and TTX-sensitive outward Cs^+/K^+ currents were observed in the other (17) cells. The time- and voltage-dependent properties of the TTX-sensitive inward Ca^{2+} and outward Cs^+/K^+ currents recorded in Nav1.5-expressing tsA-201 were indistinguishable from native currents in mouse and human cardiac myocytes. Overall, the results presented here suggest marked regional, cell type-specific, differences in the relative ion selectivity, and likely the molecular architecture, of native *SCN5A*/*Scn5a*- (Nav1.5-) encoded cardiac Na^+ channels in mouse and human ventricles.

ARTICLE HISTORY

Received 11 April 2018
Revised 27 December 2018
Accepted 2 January 2019

KEYWORDS


Left ventricles (LV);
interventricular septum; LV
endocardium; LV
epicardium; voltage-gated
 Na^+ currents; *SCN5A*; Nav1.5

Introduction

Inward calcium (Ca^{2+}) currents that are sensitive to the voltage-gated sodium (Na^+) channel toxin, tetrodotoxin (TTX), $I_{\text{Ca}(\text{TTX})}$, have been described in neuronal [1–3] and cardiac [4–7] cells. In the heart, $I_{\text{Ca}(\text{TTX})}$ has been reported to be present in human atrial myocytes [4] and in guinea-pig [5,8], rat [6,9–11], and mouse [12] ventricular myocytes. In addition to much lower amplitudes/densities than TTX-sensitive cardiac Na^+ currents, $I_{\text{Ca}(\text{TTX})}$ displays slower activation and inactivation kinetics and apparent reversal potentials (values between -35 and $+5$ mV have been reported) that are more hyperpolarized than the reversal potentials (of $+35$ to $+40$ mV) typically reported for cardiac Na^+ currents [4–6,8–11]. In some preparations, TTX-sensitive outward cesium (Cs^+) currents have also been reported and suggested to underlie some of the variability in the amplitudes/densities and the measured reversal potentials of $I_{\text{Ca}(\text{TTX})}$ [1,6,9,10].

Although widely observed, the reported amplitudes/densities and detailed time- and voltage-dependent properties of the currents are quite heterogeneous, and it has been unclear if $I_{\text{Ca}(\text{TTX})}$ is a ubiquitous feature of the myocardium or, rather displays regional variations in expression, as observed with other cardiac ion channels, particularly voltage-gated K^+ channels [13,14]. It has also been unclear if cardiac $I_{\text{Ca}(\text{TTX})}$ reflects inward Ca^{2+} flux through Na^+ channels generated by the predominant cardiac voltage-gated Na^+ channel pore-forming (α) subunit Nav1.5, encoded by *SCN5A*/*Scn5a*, or perhaps the expression and functioning of another Nav α subunit. Interestingly, in addition to Nav1.5 (*SCN5A*/*Scn5a*) several Nav α subunits, including Nav1.1 (*SCN1A*/*Scn1a*), Nav1.2 (*SCN2A*/*Scn2a*), Nav1.3 (*SCN3A*/*Scn3a*), Nav1.4 (*SCN4A*/*Scn4a*) and Nav1.6 (*SCN8A*/*Scn8a*) have been reported to be expressed in mammalian cardiac myocytes [15–18], albeit at much lower densities

CONTACT C. William Balke  bill.balke@wustl.edu; jnerbonne@wustl.edu

 Supplementary data for this article can be [here](#).

© 2019 The Author(s). Published by Informa UK Limited, trading as Taylor & Francis Group.

This is an Open Access article distributed under the terms of the Creative Commons Attribution License (<http://creativecommons.org/licenses/by/4.0/>), which permits unrestricted use, distribution, and reproduction in any medium, provided the original work is properly cited.

than Nav1.5. Nevertheless, these traditionally considered “non-cardiac” Nav α subunits are differentially expressed in the myocardium and have been suggested to play roles in the generation of cardiac Nav currents [15–19]. Previous studies focused on defining the molecular determinants of $I_{Ca(TTX)}$, however, have provided conflicting results. It has, for example, been proposed that Nav1.5-encoded channels underlie $I_{Ca(TTX)}$ [5,7,10]. In marked contrast, the results of experiments conducted on adult rat ventricular cells incubated with an antisense oligonucleotide directed against rat *Scn5a* have been interpreted as suggesting that a different (i.e. not Nav1.5) Nav α subunit underlies $I_{Ca(TTX)}$ [20]. It has also been suggested, however, that voltage-gated cardiac Ca^{2+} channels, both high threshold, L-type Ca^{2+} channels [21–23] and low threshold, T-type Ca^{2+} channels [8,24], contribute to $I_{Ca(TTX)}$.

In the experiments here, we used a combination of electrophysiological and pharmacological approaches to test the hypothesis that $I_{Ca(TTX)}$ is differentially expressed in native (mouse and human) ventricular myocardium. These experiments revealed marked differences in the densities of $I_{Ca(TTX)}$ and of TTX-sensitive outward Cs^+/K^+ currents in myocytes isolated from adult mouse interventricular septum (IVS), left ventricular (LV) endocardium, apex, and epicardium, as well as in human LV endocardial and epicardial myocytes. In addition, we present the results of experiments conducted on heterologously expressed human *SCN5A*- (Nav1.5-) encoded Na^+ channels that suggest that *both* $I_{Ca(TTX)}$ and TTX-sensitive outward currents are generated by Nav1.5 (*SCN5A/Scn5a*) in mouse and human ventricular myocytes.

Methods

Ethical approvals

Animals were handled in accordance with the NIH Guide for the Care and Use of Laboratory Animals (NIH publication No. 85–23). All protocols involving animals were approved (Approval number 20140268) by the Animal Studies Committee at Washington University Medical School. Experiments were performed on adult (age range 9–15 week) male and female wild type (WT) C57BL6/J mice (Jackson Laboratory, Bar Harbor, ME).

Non-failing adult (age range 38–74 years; mean 59 ± 5 years) male ($n = 5$) and female ($n = 2$) human hearts, declined for transplantation, were obtained from Mid-America Transplant Services (St. Louis, MO). Approval (IRB ID# 201105210) for the use of human tissues was obtained from the Washington University in St. Louis Institutional Review Board (Washington University, St. Louis Department of Health & Human Services Federal Wide Assurance #FWA00002284), with a full HIPAA waiver.

Isolation of mouse ventricular myocytes

Myocytes were isolated from adult (9–15-week-old) male and female C57BL6/J mice by enzymatic dissociation and mechanical dispersion using previously described methods [25,26]. Briefly, hearts were removed from anaesthetized (Avertin; 0.25 mg kg^{-1} , I.P.; Sigma, St Louis, MO, USA) mice, mounted on a Langendorff apparatus, and perfused retrogradely through the aorta with 25 ml of a Ca^{2+} -free Hepes-buffered Eagle’s balanced salt solution (Gibco/Invitrogen, Carlsbad, CA) supplemented with 6 mM glucose, amino acids and vitamins, followed by 25 ml of the same buffered solution containing (0.8 mg ml^{-1}) Type II collagenase (Worthington Biochemical Corp., Lakewood, NJ) at 37°C for 15–20 min. Following the perfusion, the interventricular septum, left ventricular (LV) free wall and the LV apex were separated using a fine scalpel and iridectomy scissors; in some experiments, the endocardial and epicardial surfaces of the LV free wall were dissected. Tissue pieces were minced and incubated (separately) for 5 min in fresh enzyme-free buffer containing bovine serum albumin (5 mg ml^{-1} ; Sigma) and taurine (1.2 mg ml^{-1} ; Sigma) and subsequently dispersed by gentle trituration. The resulting cell suspensions were filtered. Cells were harvested by gravity sedimentation and resuspended in serum-free medium-199 (M-199; Sigma). Isolated myocytes were plated on laminin (Sigma) coated glass coverslips and maintained in a 95% air-5% CO_2 incubator at 37°C for at least 1 h before using in electrophysiological experiments. Whole-cell recordings were obtained at room temperature ($22 \sim 24^\circ\text{C}$) from mouse myocytes within 24 h of cell isolation.

Isolation of human ventricular myocytes

Non-failing human hearts ($n = 7$; mean \pm SEM age = 59 ± 5 years), deemed not suitable for transplantation for technical or non-cardiac reasons, were obtained from Mid-America Transplant Services). In each case, a transmural wedge of the left ventricle (LV), including a piece of the left anterior descending (LAD) artery, was excised. A surface branch of the LAD was cannulated and perfused with oxygenated Krebs buffer containing (in mM): 118 NaCl, 4.8 KCl, 1.2 MgCl₂, 1.2 KH₂PO₄, 25 NaHCO₃, 11 Glucose, 1.8 CaCl₂, 0.01 Phenol Red, pH 7.3 at 37°C for 20 min. Wedges were subsequently perfused with Ca²⁺-free Krebs buffer supplemented with essential amino acids except L-glutamine (Gibco/Invitrogen), 1.5 nM insulin (Sigma), and 0.03 mM EGTA for ~15 min, before perfusion of supplemented Krebs buffer containing 35 μ M CaCl₂ and 0.5–0.7 mg/ml of Type II collagenase (Worthington) at 37°C. Following 20 min perfusion of the enzyme-containing solution, Mayo scissors were used to remove the epicardial (LV epi) and endocardial (LV endo) regions of the LV free wall; these were minced and incubated (separately) in fresh collagenase-containing solution for an additional 15 min at 37°C. Following trituration, the resulting cell suspensions were filtered and resuspended in serum-free M-199 (Sigma). Isolated myocytes were plated on laminin-coated coverslips and maintained in a 95% air-5%CO₂ incubator at 37°C for at least 1 h before using in electrophysiological experiments. Whole-cell recordings were obtained at room temperature (22 ~ 24°C) from human LV myocytes within 24 h of cell isolation.

Heterologous expression of human Nav1.5

tsA-201 cells, obtained from the American Tissue Culture Collection (Manassas, VA), were maintained in Dulbecco's Modified Eagle Medium (Gibco/Invitrogen), supplemented with 5% horse serum (Gibco/Invitrogen), 5% heat-inactivated fetal calf serum (Gibco/Invitrogen) and 1 unit/ml penicillin-streptomycin (Gibco/Invitrogen), in a 95% air-5%CO₂ incubator at 37°C. Cells were passaged at confluence every 2–3 days by brief trypsinization. For electrophysiological recordings, tsA-201 cells were plated on 35 mm tissue culture (plastic) dishes

at low density and transfected *in situ*. For transfections, 0.2 μ g of an enhanced green fluorescent protein- (eGFP-) expressing plasmid alone, or 2 μ g of a human SCN5A- (Nav1.5-) expressing and 0.2 μ g of the eGFP-expressing plasmid, was mixed with 2 μ g Lipofectamine 2000 (Life Technologies Inc., Gaithersburg, MD) in Opti-MEM (Gibco/Invitrogen), incubated at room temperature for ~30 min, and subsequently added to the tissue culture dishes containing tsA-201 cells, maintained in a 95% air-5%CO₂ incubator at 37°C. Approximately 8 h later, the plasmid-containing solutions were replaced with normal cell culture medium (see above). eGFP expression was identified under epifluorescence illumination 24–36 h after transfections, and electrophysiological recordings were obtained from eGFP-expressing cells.

Electrophysiological recordings

Whole-cell voltage-clamp recordings were obtained at room temperature (22–24°C) from mouse and human ventricular myocytes within 24 hr of isolation and from transfected tsA-201 cells using a Dagan 3900A (Dagan Corporation) amplifier, interfaced to a Digidata 1332A A/D converter (Molecular Devices) and pClamp 10.3 (Molecular Devices). Recording pipettes routinely contained (in mmolL⁻¹): 120 glutamic acid, 120 CsOH, 10 HEPES, 0.33 MgCl₂, 20 tetraethylammonium chloride (TEA-Cl), 4 Mg-ATP, and 5 EGTA (pH adjusted to 7.3 with CsOH) [6]. In some experiments, N-methyl-D-glucamine (NMDG⁺) was used in place of the Cs⁺ (to eliminate the outward currents through TTX-sensitive channels; the pipette solution contained (in mM): 150 NMDG⁺, 4 Mg-ATP and 5 EGTA (pH adjusted to 7.3 with HCl/Tris base). In experiments focused on recording outward K⁺ currents, pipettes contained (in mmolL⁻¹): 135 KCl, 10 EGTA, 10 HEPES, 5 glucose, 5 K₂ATP (pH adjusted to 7.2 with KOH) [27]. Pipette resistances were 1.5–2.0 M Ω when filled with either recording solution. In all experiments, junction potentials were compensated prior to seal formation.

Electrophysiological data were acquired at 10–20 kHz and signals were low-pass filtered at 5 kHz before digitization and storage. After the formation of

a giga-seal ($> 1 \text{ G}\Omega$) and establishment of the whole-cell configuration, brief (10 ms) $\pm 10 \text{ mV}$ voltage steps from a holding potential of -70 mV were presented to allow measurements of whole-cell membrane capacitances (C_m), input resistances (R_{in}) and series resistances (R_s). The mean \pm SEM C_m and R_{in} determined for mouse ventricular myocytes were $156 \pm 6 \text{ pF}$ and $997 \pm 184 \text{ M}\Omega$ ($n = 94$) and, for human ventricular myocytes, were $162 \pm 20 \text{ pF}$ and $1354 \pm 309 \text{ M}\Omega$ ($n = 26$). In each cell, C_m and R_s were compensated by $\geq 85\%$; voltage errors resulting from uncompensated series resistance were always $< 2 \text{ mV}$ and were not corrected. Leak currents were always $< 50 \text{ pA}$ and were not corrected.

Cells were initially superfused (rate $2\text{--}3 \text{ ml min}^{-1}$) with a 0 mM Na^+ bath solution containing (in mmolL^{-1}): 140 TEA-Cl , 10 CsCl , 1 MgCl_2 , 2 CaCl_2 , 10 HEPES and 10 glucose (pH adjusted to 7.4 with CsOH) [6]. In some experiments, NMDG^+ replaced the TEA-Cl in the bath solution; the NMDG^+ bath solution contained (in mM): 150 NMDG^+ , 1 MgCl_2 , 2 CaCl_2 , 10 HEPES and 10 glucose (pH adjusted to 7.4 with HCl/Tris base). Whole-cell inward and outward currents, evoked in response to 300 ms voltage steps to potentials between -90 and $+25 \text{ mV}$ from a HP of -50 mV and -100 mV , were recorded; depolarizing voltage steps were presented in 5 mV increments at 2 s intervals. A multi-manifold perfusion system [27] was used to apply bath solutions of varying Na^+ and/or Ca^{2+} concentrations, as well as the Tetrodotoxin- (TTX -; Alomone labs, Jerusalem), the Ni^{2+} - (NiCl_2 ; Sigma), the verapamil- (verapamil hydrochloride; Sigma) and the 2-aminoethyl methanesulfonate hydrochloride- (MTSEA -; MTSEA-Cl (US Biologicals, San Diego, CA) containing bath solutions during recordings.

MTSEA-Cl was dissolved in dimethyl sulfoxide (DMSO) and diluted in bath solution to a final concentration of 2 mM ; control experiments revealed that the DMSO (0.1%) in the MTSEA -containing bath solution did not measurably affect the passive membrane properties of myocytes or the amplitudes/properties of voltage-dependent currents. The waveforms of the TTX -sensitive currents were obtained by off-line digital subtraction of records obtained in the presence of TTX from the controls.

Data analysis and statistics

Electrophysiological data were compiled and analyzed using Clampfit 10.3 (Molecular Devices) and GraphPad (Prism). Peak inward/outward current amplitudes were measured in each cell at various test potentials and normalized to the whole-cell membrane capacitance (in the same cell); current densities (pA/pF) are reported. The decay phases of currents ($I_{\text{Ca(TTX)}}$, I_{Na} and $I_{\text{Ca,L}}$) were fitted by one ($y(t) = A \cdot \exp(-t/T) + B$) exponential (for $I_{\text{Ca(TTX)}}$) or two ($y(t) = A_{\text{fast}} \cdot \exp(-t/T_{\text{fast}}) + A_{\text{slow}} \cdot \exp(-t/T_{\text{slow}}) + B$) exponentials (for I_{Na} and $I_{\text{Ca,L}}$), where T , T_{fast} and T_{slow} are the decay time constants, A , A_{fast} and A_{slow} are the amplitudes of the inactivating current components, and, in each case, B corresponds to the steady-state component of the total current. The voltage-dependences of activation of the peak inward currents through Nav1.5-encoded channels were determined by first measuring the peak amplitudes of the currents evoked at various test potentials from a holding potential of -100 mV . Conductances (G_{Na}) were calculated and normalized to the maximal conductance ($G_{\text{Na,max}}$) determined in the same cell. Mean \pm SEM normalized conductances ($G_{\text{Na}}/G_{\text{Na,max}}$) were then plotted as a function of the test potential and fitted with a Boltzmann equation: $G_{\text{Na}} = G_{\text{Na,max}} / [1 + \exp((V_{1/2} - V)/k)]$, where $G_{\text{Na,max}}$ is the maximal conductance, V is the test potential, $V_{1/2}$ is the potential of half maximal activation, and k is the slope factor. All data are presented as means \pm SEM. The statistical significance of observed differences was evaluated using a paired (compared in the same cell) two-tailed student's t test, one-way or two-way ANOVA, as indicated in the text or figure legends; P values ≤ 0.05 were considered statistically significant.

Results

Ttx-sensitive inward Ca^{2+} currents in mouse interventricular septum myocytes

Whole-cell voltage-clamp recordings, obtained from isolated mouse interventricular septum (IVS) myocytes with 2 mM Ca^{2+} and 0 mM Na^+ in the bath solution and 120 mM Cs^+ in the recording pipettes, revealed two distinct inward current components. As illustrated in the representative

recordings presented in Figure 1(a) (panel a), a rapidly activating and inactivating inward current (arrow in panel a) was observed on membrane depolarizations from a holding potential (HP) of -100 mV to the more hyperpolarized (e.g. -55 mV to -25 mV) test potentials, followed by a more slowly activating and inactivating current at the more depolarized membrane potentials. Only the more slowly activating/inactivating current was observed when the currents were evoked from a HP of -50 mV (Figure 1(a), panel b), consistent with the presence of a high threshold voltage-gated inward cardiac Ca^{2+} current [28–30], now typically referred to as I_{Ca} “long lasting” or $I_{\text{Ca,L}}$ [23,31]. The rapidly activating and inactivating component of the inward Ca^{2+} current was isolated by off-line digital subtraction of the currents evoked from -50 mV from those evoked from -100 mV (Figure 1(a), panel c). Peak inward Ca^{2+} current densities evoked from -100 mV (\bullet) and -50 mV (\square) in this cell, are plotted as a function of the test potential in Figure 1(c). The current component seen only on depolarizations from a HP of -100 mV (\bullet) is indicated by the arrow.

Additional experiments revealed that the rapidly activating and inactivating component of the inward Ca^{2+} current in mouse IVS myocytes is selectively blocked (Figure 1(b)) by μM concentrations of the Na^+ channel selective toxin, tetrodotoxin (TTX). As illustrated in Figure 1(b), panel b, bath application of $10 \mu\text{M}$ TTX eliminated the low threshold, rapidly activating and inactivating component of the inward Ca^{2+} current without measurably affecting the slowly activating and inactivating Ca^{2+} current, $I_{\text{Ca,L}}$. The current-voltage relation for $I_{\text{Ca,L}}$ (Figure 1(b), panel b), evoked from -100 mV in the presence of $10 \mu\text{M}$ TTX (\blacktriangle), is plotted in C. Offline digital subtraction of the inward currents evoked from a HP of -100 mV in the presence of TTX (Figure 1(b), panel b), from those recorded in the absence of TTX (Figure 1(b), panel a) revealed the TTX-sensitive component of I_{Ca} (Figure 1(b), panel c), similar to TTX-sensitive inward Ca^{2+} currents previously described in cardiac myocytes from several species that have been referred to as $I_{\text{Ca(TTX)}}$ [5–7,9,10,12,20].

Although low threshold, “T” type, Ca^{2+} channels [32] have previously been identified in mammalian cardiac myocytes [29], additional experiments revealed that the rapidly activating and inactivating

inward Ca^{2+} current component evoked from a holding potential of -100 mV in isolated mouse IVS myocytes is not affected by the selective T-type Ca^{2+} channel blocker Ni^{2+} (Figure 1(d)) at $100 \mu\text{M}$, suggesting that the TTX-sensitive inward Ca^{2+} current does not reflect Ca^{2+} entry through T-type Ca^{2+} channels. In addition, although the high threshold, slowly activating and inactivating Ca^{2+} current component is reduced by the selective L-type Ca^{2+} channel blocker verapamil [33] in a dose-dependent manner (Figure 1(e)), verapamil does not measurably affect the low threshold, rapidly activating and inactivating TTX-sensitive component of the inward Ca^{2+} current that we refer to as $I_{\text{Ca(TTX)}}$.

Using the protocol illustrated in Figure 1 B, $I_{\text{Ca(TTX)}}$ was identified in all mouse IVS myocytes ($n = 20$) examined, although there was, as is illustrated in Figure 2, considerable variability in peak inward current amplitudes/densities among cells (Figure 2(b)). In addition, in 8 of the 20 IVS cells studied using this protocol, outward (Cs^+) currents were observed at -25 mV (Figure 2(b)). The mean \pm SEM peak TTX-sensitive current densities measured from recordings obtained from mouse IVS cells ($n = 20$) during voltage-steps to potentials between -90 and -25 mV (in 5 mV increments) are plotted as a function of test potential in Figure 2(c); at more positive (≥ -20 mV) test potentials, the mean \pm SEM peak currents were outward.

$I_{\text{Ca(TTX)}}$ is blocked by MTSEA, a selective antagonist of Nav1.5-encoded Na^+ channels

Addition of (2 mM) MTSEA, a selective inhibitor of Nav1.5-encoded cardiac Na^+ channels [19,34,35] to the bath solution eliminated $I_{\text{Ca(TTX)}}$ in mouse IVS myocytes. As illustrated in the representative recordings obtained from a mouse IVS cell presented in Figure 3(a), inward Ca^{2+} currents were recorded under control conditions with 2 mM Ca^{2+} and 0 mM Na^+ in the bath and 120 mM Cs^+ in the recording pipette (left panel). When the bath solution was switched to one containing 2 mM MTSEA, the currents were eliminated (Figure 3(a), right panel). Similar results were obtained in experiments on 14 adult mouse IVS myocytes and the mean \pm SEM ($n = 14$) current-voltage relations determined for these cells

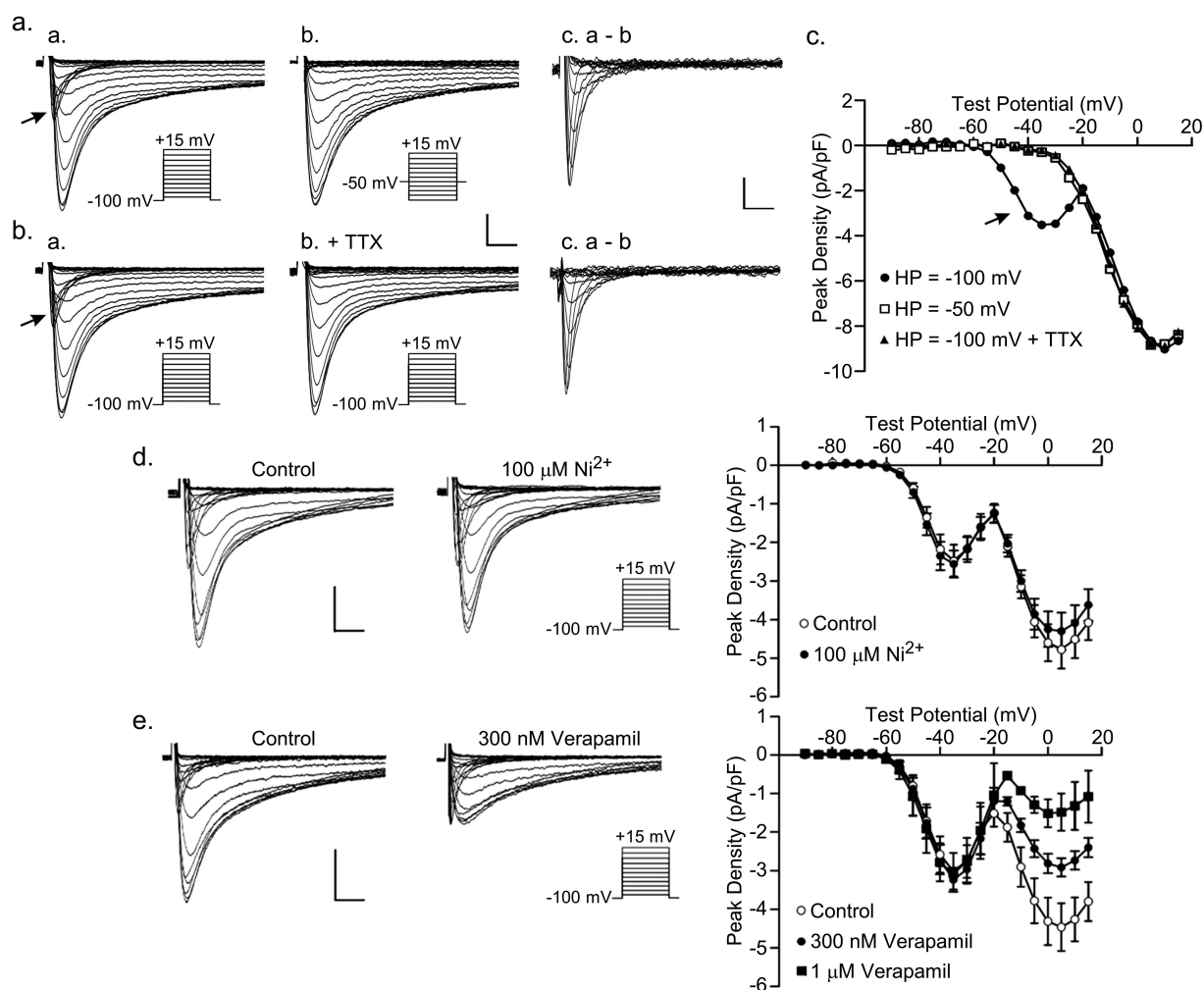


Figure 1. TTX-sensitive Ca^{2+} currents in mouse interventricular septum (IVS) myocytes. Voltage-gated inward Ca^{2+} currents (I_{Ca}) in mouse IVS myocytes were measured with 2 mM Ca^{2+} and 0 mM Na^+ in the bath (see Methods) and 120 mM Cs^+ in the recording pipettes. (a) Representative I_{Ca} elicited in an IVS myocyte in response to 300 ms voltage steps to test potentials between -90 and $+15$ mV (in 5 mV increments) from a holding potential (HP) of -100 mV, are shown in panel a; currents evoked in the same cell from a HP of -50 mV are shown in panel b. The rapidly activating and inactivating component of I_{Ca} (arrow in panel a) is not evident in the records evoked from -50 mV (panel b). The waveforms of this component, obtained by off-line digital subtraction of the currents evoked at test potentials between -90 mV and -25 mV from a HP of -50 mV from those evoked from a HP of -100 mV, are shown in panel c. (b) In the same cell as in (a), currents evoked from -100 mV were recorded before (panel a) and after (panel b) the addition of $10 \mu\text{M}$ TTX to the bath. The waveforms of the TTX-sensitive Ca^{2+} current ($I_{\text{Ca(TTX)}}$), obtained by off-line digital subtraction of the currents recorded at test potentials between -90 mV and -25 mV in the absence (panel a) and presence (panel b) of TTX, are shown in panel c. In (a) and (b), the scale bars are 2 pA/pF and 10 ms in panels a and b, and 1 pA/pF and 10 ms in panel c. (c) Peak inward Ca^+ currents evoked from -100 mV in the absence (●) and the presence (▲) of TTX and from -50 mV (□) are plotted as a function of the test potential; the arrow indicates the TTX-sensitive inward Ca^+ current, $I_{\text{Ca(TTX)}}$. (d) Representative I_{Ca} elicited in an IVS myocyte using the same voltage-clamp protocol (illustrated adjacent to the current records) as in (b), before and after exposure to the $100 \mu\text{M}$ Ni^{2+} -containing bath solution; scale bars are 2 pA/pF and 10 ms. Similar results were obtained on 6 cells. Mean \pm peak inward Ca^+ current densities evoked from -100 mV before (○) and after (●) the application of the $100 \mu\text{M}$ Ni^{2+} -containing bath solution are plotted as a function of the test potential in the panel on the right. (E) Representative I_{Ca} elicited in an IVS myocyte before (○) and after (●) the application of the 300 nM verapamil-containing bath solution; scale bars are 2 pA/pF and 10 ms. Similar results were obtained on 4 cells. Mean \pm peak inward Ca^+ current densities evoked from -100 mV in control bath (○) and following exposure to the 300 nM (●) or the $1 \mu\text{M}$ (■) verapamil-containing bath solution are plotted as a function of the test potential in the panel on the right.

before (●) and after (○) exposure to 2 mM MTSEA are plotted in Figure 3(b); no inward or outward currents were recorded in the presence of 2 mM MTSEA.

When recordings were obtained from isolated adult mouse IVS myocytes with increased (from 0 mM to 20 mM) Na^+ in the bath, much larger amplitude inward (Na^+) currents were observed

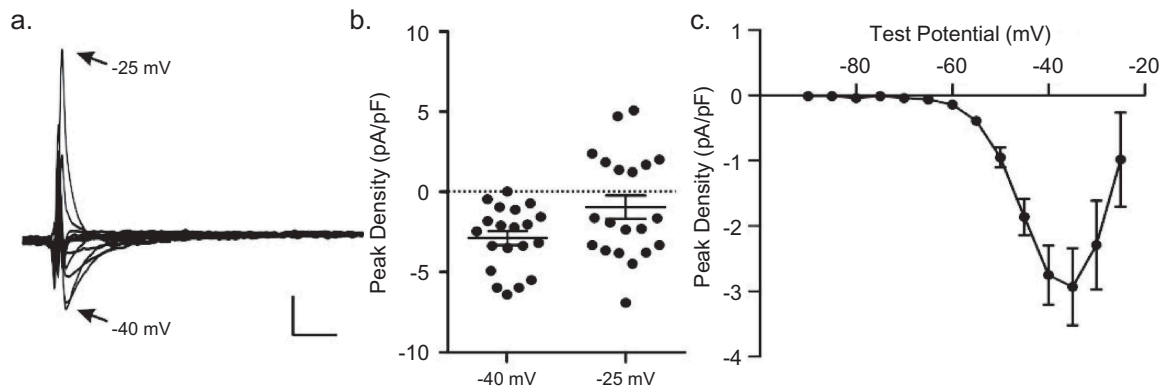


Figure 2. Heterogeneous expression of $I_{Ca(TTX)}$ in mouse IVS myocytes. Whole-cell currents, elicited in response to 300 ms voltage steps to test potentials between -90 and -25 mV (in 5 mV increments) from a HP of -100 mV, were recorded from mouse IVS myocytes ($n = 20$) with 2 mM Ca^{2+} /0 mM Na^{+} in the bath and 120 mM Cs^{+} in the pipettes before and after application of 10 μ M TTX, as described in the legend to Figure 1. (a) The waveforms of the TTX-sensitive currents, obtained by off-line digital subtraction of the records in the absence and presence of 10 μ M TTX, in one of these IVS cells is shown; the scale bars are 1 pA/pF and 10 ms. The currents evoked at test potentials of -40 mV (\bullet) and -25 mV (\bullet) are indicated. (b) The peak current densities at -40 mV and -25 mV in individual IVS cells ($n = 14$) are plotted. (c) Mean \pm SEM (\bullet ; $n = 20$) peak TTX-sensitive current densities in mouse IVS cells are plotted as a function of test potential; the mean \pm SEM extrapolated reversal potential of the TTX-sensitive currents in mouse IVS myocytes was -18.1 ± 3.7 mV.

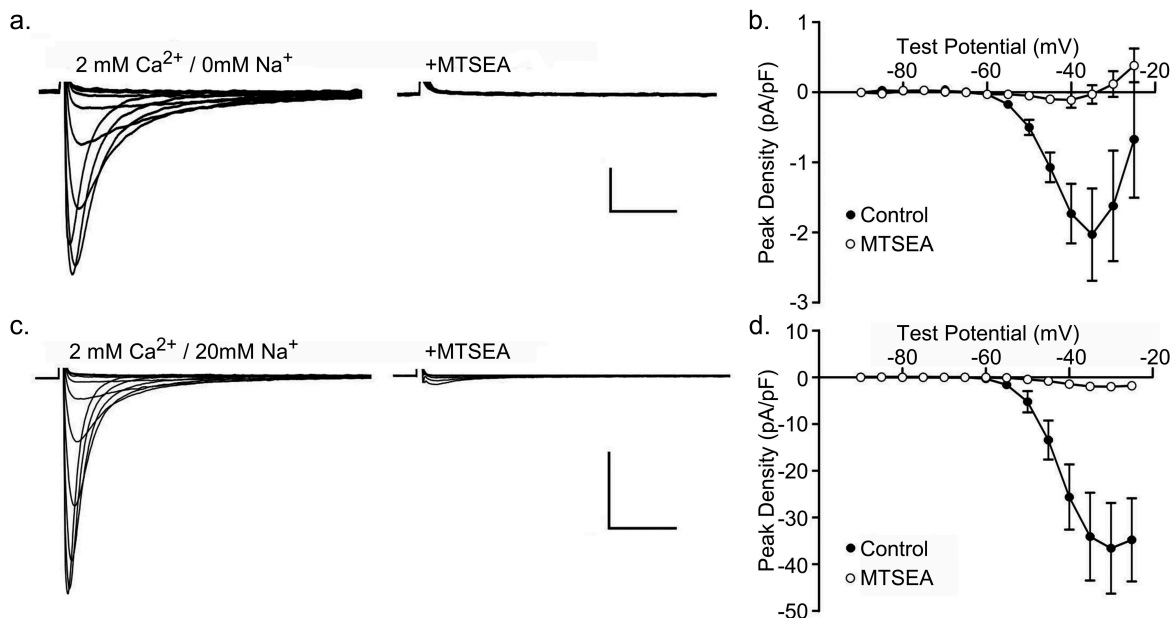


Figure 3. MTSEA blocks TTX-sensitive inward Ca^{2+} currents in mouse IVS myocytes. (a) With 2 mM Ca^{2+} /0 mM Na^{+} in the bath and 120 mM Cs^{+} in the pipette, $I_{Ca(TTX)}$ was recorded in a mouse IVS cell as described in the legend to Figure 2. On application of 2 mM MTSEA, the currents were eliminated; scale bars are 1 pA/pF and 10 ms. (b) Mean \pm SEM peak current densities measured in mouse IVS myocytes ($n = 14$) before (\bullet) and after (\circ) application of the MTSEA-containing bath solution are plotted as a function of the test potential. (c) Robust inward Na^{+} currents (I_{Na}) were recorded from isolated mouse IVS myocytes with bath solution containing 2 mM Ca^{2+} /20 mM Na^{+} and 120 mM Cs^{+} in the pipette. Similar to $I_{Ca(TTX)}$ (a), I_{Na} was also eliminated on perfusion of 2 mM MTSEA-containing bath solution (c). Scale bars are 10 pA/pF and 10 ms. (d) Mean \pm SEM ($n = 4$) peak current densities in IVS myocytes with 2 mM Ca^{2+} /20 mM Na^{+} in the bath before (\bullet) and after (\circ) MTSEA are plotted as a function of the test potential.

(Figure 3(c), left panel); note the different scale bar in Figure 3(c), compared with Figure 3(a). Application of 2 mM MTSEA also eliminated the inward Na^{+} currents (Figure 3(c), right panel). The mean \pm SEM ($n = 4$) current-voltage

relations for the peak currents recorded in isolated mouse IVS cells with 20 mM Na^{+} and 2 mM Ca^{2+} in the bath, before (\bullet) and after (\circ) the application of 2 mM MTSEA are presented in Figure 3(d).

Regional differences in expression of TTX-sensitive inward Ca^{2+} and outward Cs^+ currents in adult mouse ventricles

Additional experiments were completed to quantify the expression of TTX-sensitive inward/outward currents in myocytes isolated from different regions of adult mouse left ventricles (LV). As in the experiments on mouse IVS myocytes, voltage-activated inward/outward currents, evoked from a HP of -100 mV in response to 300 ms test potentials between -90 mV to -25 mV (in 5 mV increments) were recorded with 2 mM Ca^{2+} /0 mM Na^+ in the bath and 120 mM Cs^+ in the recording pipettes, before and after the addition of 10 μM TTX. Representative recordings of the TTX-sensitive currents obtained from myocytes isolated from the LV endocardium (LV Endo, panel a), LV epicardium (LV Epi, panel b) and LV apex (LV Apex, panel c) are presented in Figure 4(a); note that the scale bars are different in panels a (0.5 pA/pF), b and c (1.0 pA/pF). The peak TTX-sensitive inward/outward current densities measured in individual adult mouse LV Endo (\blacktriangle ; $n = 11$), LV Epi (\blacksquare ; $n = 8$) and LV apex (\blacklozenge ; $n = 11$) myocytes at test potentials of -40 mV and -25 mV are presented in Figure 4(b)). Mean \pm SEM peak TTX-sensitive current densities in adult mouse LV Endo (\blacktriangle ; $n = 11$), LV Epi (\blacksquare ; $n = 8$) and LV apex (\blacklozenge ; $n = 11$) myocytes are plotted as a function of test potential in Figure 4(c).

Although prominent outward Cs^+ currents were recorded in cells from all three regions of the adult mouse LV, outward currents were larger in LV epi and LV apex myocytes, and inward $I_{\text{Ca}(\text{TTX})}$ was only evident in recordings from LV endo cells (Figure 4(a), panel a). The mean \pm SEM peak $I_{\text{Ca}(\text{TTX})}$ density (at -40 mV) in LV endo cells of -0.9 ± 0.5 pA/pF ($n = 11$), however, was much lower than the mean \pm SEM peak $I_{\text{Ca}(\text{TTX})}$ density (at -40 mV) of (-2.9 ± 0.5) pA/pF ($n = 20$) measured in IVS myocytes. Similar results were obtained when 120 mM K^+ replaced the Cs^+ in the recording pipettes (data not shown). These combined observations suggested the interesting hypothesis and that inward TTX-sensitive Ca^{2+} currents might be revealed in mouse LV apex (and LV epi) myocytes if the outward Cs^+/K^+ currents were blocked. To test this hypothesis,

additional experiments were conducted with NMDG⁺, which does not permeate voltage-gated Na^+ channels [10], used in place of the Cs^+/K^+ , in the recording pipettes. As illustrated in Figure 4(d), TTX-sensitive inward Ca^{2+} currents were recorded from LV apex and, as expected, from IVS myocytes with NMDG⁺-containing pipette solution (see: **Methods**). In addition, although the mean \pm SEM amplitudes/densities of the currents are different, the voltage-dependent properties of $I_{\text{Ca}(\text{TTX})}$ recorded in IVS and LV apex myocytes with the NMDG⁺-containing pipette solution are indistinguishable (Figure 4(e)).

Ionic dependence of TTX-sensitive inward currents in mouse IVS myocytes

Additional experiments were conducted to compare the effects of extracellular Ca^{2+} and Na^+ on the time and voltage-dependent properties of TTX-sensitive inward currents in mouse IVS myocytes. Currents, evoked during voltage steps to test potentials between -90 mV and -25 mV from a HP of -100 mV and from a HP of -50 mV, were recorded in isolated adult mouse IVS myocytes with 2 mM Ca^{2+} /0 mM Na^+ in the bath and 120 mM Cs^+ in the recording pipettes. The bath solution was then changed sequentially to one containing 2 mM Ca^{2+} /10 mM Na^+ , followed by 2 mM Ca^{2+} /20 mM Na^+ and, finally, 0 mM Ca^{2+} /20 mM Na^+ , and the voltage-clamp paradigms were repeated. The rapidly activating and inactivating inward currents under each recording condition, isolated by off-line digital subtraction of the currents evoked from -50 mV from those evoked from -100 mV, are presented in Figure 5(a) (panels a-d). As illustrated, the inward current amplitude increased markedly (note the change in the scale) with the addition of 10 mM Na^+ (and 2 mM Ca^{2+}) to the bath (Figure 5(a), panel b). The time- and voltage-dependent properties of the inward currents, however, were similar to those observed with 0 Na^+ /2 mM Ca^{2+} in the bath (Figure 5(a), panel a).

Increasing the Na^+ in the bath to 20 mM (in the presence of 2 mM Ca^{2+}) further increased the peak inward current (Figure 5(a), panel c). With the removal of the Ca^{2+} (replaced with 2 mM Mg^{2+})

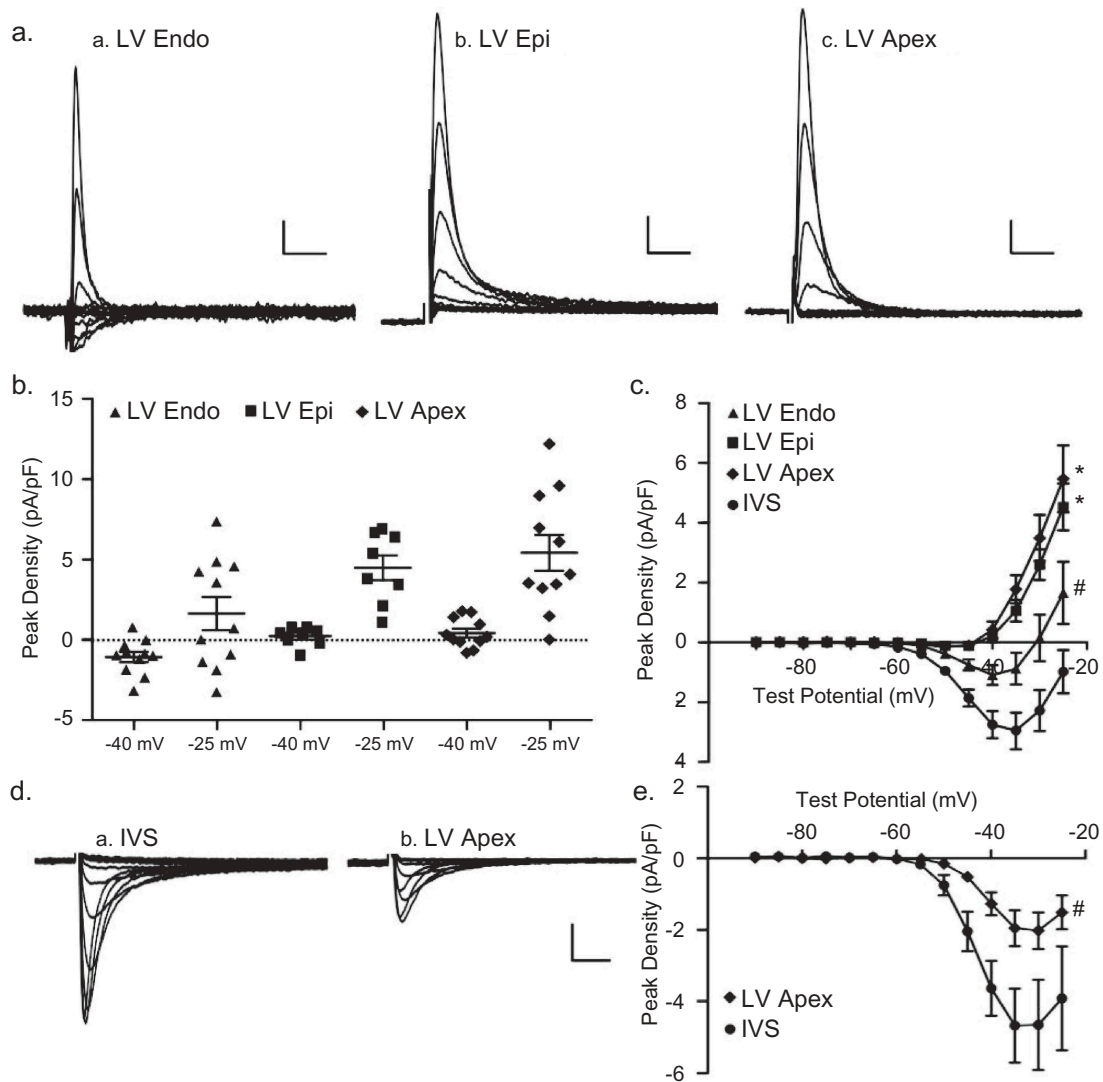


Figure 4. Regional differences in TTX-sensitive currents in adult mouse ventricles. TTX-sensitive currents were recorded and isolated as described in the legend to Figure 2 from myocytes isolated from mouse LV endocardium (LV Endo), LV epicardium (LV Epi) and LV apex. (a) Representative TTX-sensitive currents in LV Endo (panel a), LV Epi (panel b) and LV Apex (panel c) myocytes, are shown; scale bars are 0.5 pA/pF and 10 ms in panel a and 1 pA/pF and 10 ms in panels b and c. Small inward Ca^{2+} currents were seen at the more hyperpolarized test potentials in LV Endo myocytes, and outward Cs^{+} currents were recorded at the more positive test potentials. Only TTX-sensitive outward Cs^{+} currents were observed in LV Epi and LV Apex myocytes. (b) Peak densities of the TTX-sensitive currents measured at -40 mV and -25 mV in individual LV Endo (▲; $n = 11$), LV Epi (■; $n = 8$) and LV apex (◆; $n = 11$) myocytes are plotted. (c) Mean \pm SEM peak TTX-sensitive current densities measured in LV Endo (▲; $n = 11$), LV Epi (■; $n = 8$) and LV apex (◆; $n = 11$) myocytes are plotted as a function of the test potential; the mean \pm SEM peak TTX-sensitive current densities in adult mouse IVS myocytes (see Figure 2(c)) are replotted here (●) to facilitate direct comparisons of the currents across cell types. * $^{+}$ Current-voltage plots in LV Apex, LV Epi and LV Endo myocytes are significantly (two-way ANOVA) different from the current-voltage plot for the TTX-sensitive currents in IVS myocytes (●) at the $^{*}P < 0.001$ and $^{+}P < 0.05$ levels. (d) TTX-sensitive inward Ca^{2+} currents were recorded from IVS (panel a) and LV apex (panel b) myocytes with the NMDG $^{+}$ -containing pipette solution (see: **Methods**); scale bars are 2 pA/pF and 10 ms. (e) Mean \pm SEM peak TTX-sensitive inward Ca^{2+} current densities measured in IVS (●; $n = 4$) and LV apex (◆; $n = 8$) myocytes with the NMDG $^{+}$ -containing pipette solution (see: **Methods**) are plotted as a function of the test potential. Although the current-voltage plots are similar, the amplitudes/densities of the inward Ca^{2+} currents are lower ($^{+}P < 0.05$; two-way ANOVA) in mouse LV apex, compared with IVS, myocytes at all test potentials.

from the bath solution, inward current amplitudes were increased (Figure 5(a), panel d), compared with the currents recorded with 2 mM Ca^{2+} /20 mM Na^{+} (Figure 5(a), panel c). The mean \pm SEM ($n = 4$) peak

inward current versus voltage relations for the records obtained with 2 mM Ca^{2+} /0 mM Na^{+} (○), 2 mM Ca^{2+} /20 mM Na^{+} (●) and 0 mM Ca^{2+} /20 mM Na^{+} (■) in the bath were determined and are

presented in Figure 5(b). In addition to the increase in current amplitude/density, there is a marked leftward shift in the peak current-voltage plot for the records obtained with 0 mM Ca^{2+} /20 mM Na^+ (■), compared with 2 mM Ca^{2+} /20 mM Na^+ (●). The normalized voltage-dependences of activation of the inward currents recorded with 2 mM Ca^{2+} /20 mM Na^+ (●) and 0 mM Ca^{2+} /20 mM Na^+ (■) in the bath, each fitted with a single Boltzmann, are presented in Figure 5(c).

TTX-sensitive inward Ca^{2+} and outward Cs^+/k^+ currents in tsA-201 cells expressing SCN5A

Additional experiments were conducted to detail the properties of the TTX-sensitive currents expressed in tsA-201 cells transiently transfected with a plasmid encoding human SCN5A (Nav1.5) and enhanced green fluorescent protein (eGFP). Using voltage-clamp paradigms similar to those used in the experiments on mouse ventricular

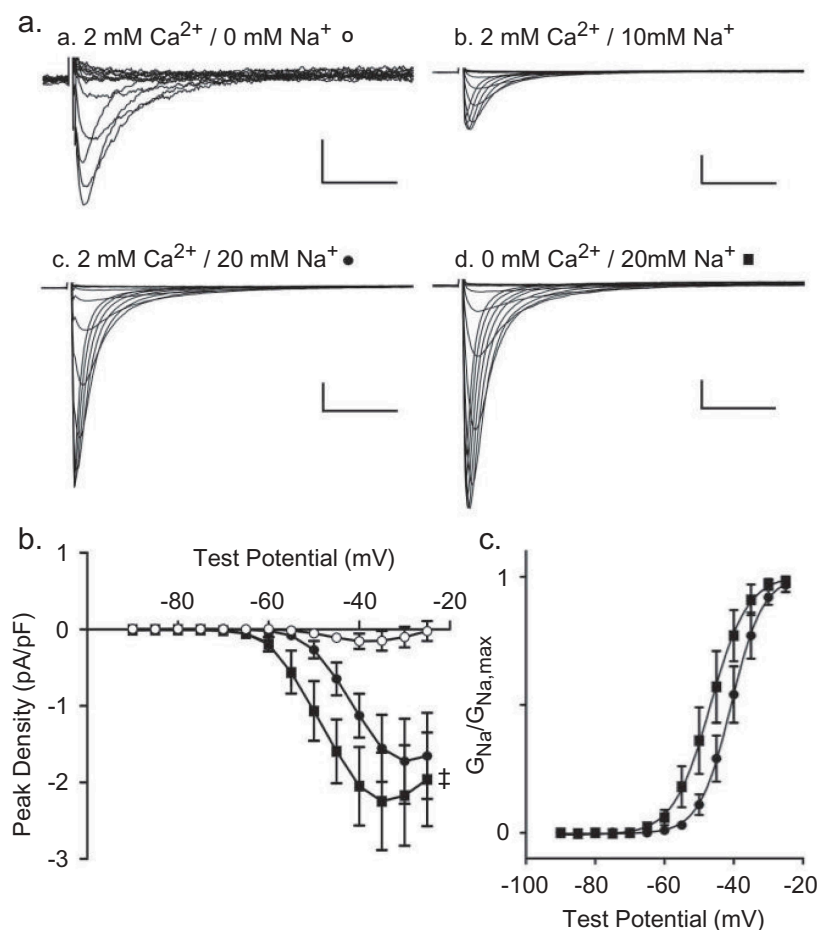


Figure 5. Extracellular Ca^{2+} modulates the voltage-dependence of Na^+ current activation in mouse IVS myocytes. Inward currents, evoked from a HP of -100 mV and from a HP of -50 mV, were recorded in mouse IVS myocytes with 2 mM Ca^{2+} /0 mM Na^+ in the bath and 120 mM Cs^+ in the recording pipettes as described in the legend to Figure 1. The bath solution was then changed sequentially to one containing 2 mM Ca^{2+} /10 mM Na^+ , 2 mM Ca^{2+} /20 mM Na^+ and 0 mM Ca^{2+} /20 mM Na^+ and the currents were again recorded (from both HPs). (a) Representative inward current waveforms recorded under these different ionic conditions, obtained by off-line digital subtraction of the currents evoked from -50 mV from those evoked from -100 mV, are illustrated. Increasing the Na^+ concentration in the bath from 0 mM (panel a; ○) to 10 mM (panel b), and further to 20 mM (panel c; ●) increased inward current amplitudes. Exchange of the extracellular solution to one containing 0 mM Ca^{2+} (replaced by 2 mM Mg^{2+}) and 20 mM Na^+ revealed in a further increase in the peak inward current amplitude (panel d; ■). Scale bars are 1 pA/pF and 10 ms in panel a and 10 pA/pF and 10 ms in panels b, c and d. (b) Similar results were obtained in 4 cells, and mean \pm SEM peak inward current densities under the different recording conditions (○, ●, ■) are plotted as a function of the test potential. The current-voltage relation was shifted ($^{\dagger}P < 0.01$; two way ANOVA) for the currents recorded with 0 mM Ca^{2+} /20 mM Na^+ (■) in the bath, compared with the currents recorded with 2 mM Ca^{2+} /20 mM Na^+ (●) in the bath. (c) Mean \pm SEM ($n = 4$) normalized voltage-dependences of activation of the peak Na^+ conductance for the currents recorded in 20 mM Na^+ and 2 mM Ca^{2+} (●) and 20 mM Na^+ and 0 Ca^{2+} (■) are plotted as a function of test potential and fitted with single Boltzmanns. The $V_{1/2}$ of current activation was shifted ($^{\dagger}P < 0.01$; paired Student's t test) to -46 ± 3 mV ($k = 4.3 \pm 0.3$), with 0 mM Ca^{2+} /20 mM Na^+ (■) in the bath, from -40 ± 2 mV ($k = 4.1 \pm 0.5$), with 2 mM Ca^{2+} /20 mM Na^+ (●) in the bath.

myocytes described above, currents, evoked during voltage steps to test potentials between -90 mV and -25 mV from a HP of -100 mV and from a HP of -50 mV, were recorded from eGFP-positive tsA-201 cells with 2 mM $\text{Ca}^{2+}/0$ mM Na^+ in the bath and 120 mM Cs^+ or 145 mM K^+ in the recording pipettes. The bath solution was then changed sequentially to 2 mM $\text{Ca}^{2+}/10$ mM Na^+ , followed by 2 mM $\text{Ca}^{2+}/20$ mM Na^+ and, finally, 0 mM $\text{Ca}^{2+}/20$ mM Na^+ , and the voltage-clamp paradigms were repeated. The currents obtained with offline digital subtraction of the currents evoked from -50 mV from those evoked from -100 mV were analyzed.

In three (of the 20) eGFP-positive tsA-201 cells from which recordings were obtained using the protocols described above, inward currents were observed (Figure 6(a-c)), whereas in the other 17 cells, only outward Cs^+ (K^+) were detected (see below; Figure 6(d-f)). No inward or outward currents, however, were recorded from tsA-201 cells ($n = 5$) transfected with only the eGFP-expressing (i.e. without Nav1.5) plasmid (Supplemental Figure 1). Recordings with 0 Na^+ / 2 mM Ca^{2+} in the bath from one of the Nav1.5-expressing tsA-201 cells in which inward currents were detected are presented in Figure 6(a) (panel a). Similar to the results obtained in mouse IVS myocytes (Figure 5), inward current amplitudes increased markedly (note the change in the scale) with 10 mM Na^+ (and 2 mM Ca^{2+}) in the bath (Figure 6(a), panel b), and further with 20 mM Na^+ (and 2 mM Ca^{2+}) in the bath (Figure 6(a), panel c). In addition, inward current amplitudes were further increased when the Ca^{2+} was removed (and replaced with 2 mM Mg^{2+}) from the bath (Figure 6(a), panel d). The peak inward current-voltage relations for the recordings (in A) obtained with 2 mM $\text{Ca}^{2+}/0$ mM Na^+ (o), 2 mM $\text{Ca}^{2+}/20$ mM Na^+ (●) and 0 mM $\text{Ca}^{2+}/20$ mM Na^+ (■) in the bath are presented in Figure 6(b). Similar to the results obtained in mouse IVS myocytes, the inward currents followed monoexponential decay kinetics with 0 Na^+ in the bath, but were best described by the sum of two exponentials with 20 mM Na^+ (and either 2 mM Ca^{2+} or 0 mM Ca^{2+}) in the bath (Supplemental Figure 2). Also, similar to the results in mouse IVS cells (Figure 5), the peak of the current-voltage curve (Figure 6(b)) and the

normalized conductance versus voltage plot (Figure 6(c)) are shifted in the hyperpolarizing direction for recordings obtained with 0 mM $\text{Ca}^{2+}/20$ mM Na^+ (■), compared with 2 mM $\text{Ca}^{2+}/20$ mM Na^+ (●), in the bath.

In most (17/20 cells) tsA-201 cells expressing Nav1.5, only outward currents were observed in the presence of 2 mM $\text{Ca}^{2+}/0$ mM Na^+ in the bath and 145 mM K^+ (Figure 6(d), panel a) or 120 mM Cs^+ (not shown) in the recording pipettes. With increased Na^+ (10 mM, 20 mM) in the bath, the outward currents progressively decreased and inward Na^+ currents were recorded (Figure 6(d), panels b and c). Removal of the Ca^{2+} (replaced with Mg^{2+}) from the bath further increased the inward current amplitudes (Figure 6(d), panel d). Peak outward K^+ (o), and inward Na^+ (●,■) currents are plotted as a function of test potential in Figure 6(e). The normalized conductance-voltage relations for the peak inward Na^+ currents recorded in 20 mM Na^+ and 2 mM Ca^{2+} (●) and 20 mM Na^+ and 0 Ca^{2+} (■), fitted with single Boltzmanns, are presented in Figure 6(f). Similar to the findings in myocytes (Figure 3), the TTX-sensitive inward Ca^{2+} and outward Cs^+/K^+ currents in Nav1.5-expressing tsA-201 cells were blocked by MTSEA (data not shown).

Differential expression of TTX-sensitive inward/outward currents in human LV myocytes

Whole-cell recordings were obtained from myocytes isolated from the endocardial (LV Endo) and epicardial (LV Epi) surfaces of human LV free wall (see Methods) with 2 mM Ca^{2+} and 0 mM Na^+ in the bath and 120 mM Cs^+ in the recording pipettes. Currents, evoked from a HP of -100 mV in response to 300 ms test potentials between -90 mV to -25 mV (in 5 mV increments), were recorded in the absence and in the presence of 10 μM TTX, and the TTX-sensitive currents, obtained by offline digital subtractions of the records before and after exposure to TTX, were analyzed. As illustrated in the representative records shown in Figure 7(a), small TTX-sensitive inward currents were observed in human LV Endo cells, whereas TTX-sensitive outward currents were seen in all human LV Endo (Figure 7(a), left)

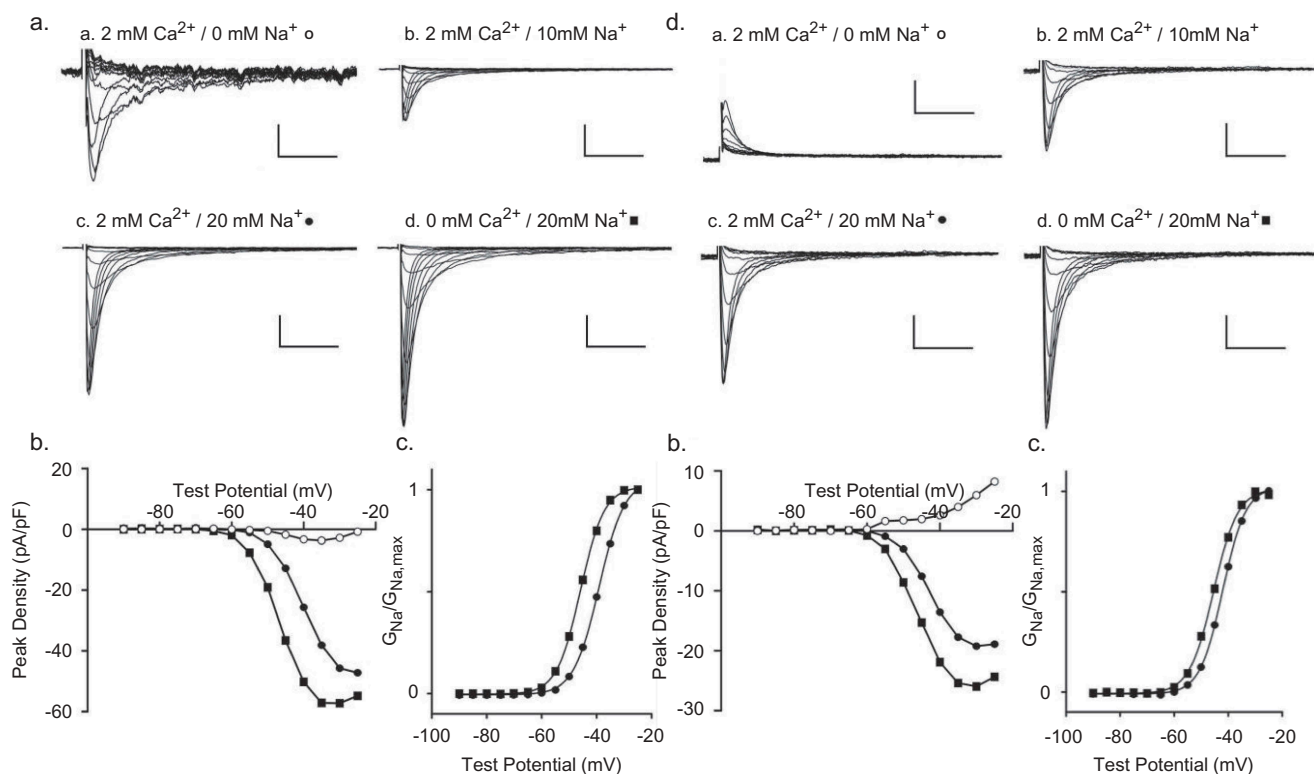


Figure 6. Inward/outward currents were also recorded from tsA-201 cells expressing SCN5A (Nav1.5). Whole-cell currents, evoked in response to 300 ms voltage steps to test potentials between -90 and -25 mV (in 5 mV increments) from -100 mV and from -50 mV with 2 mM $\text{Ca}^{2+}/0$ mM Na^{+} in the bath and 120 mM Cs^{+} (or K^{+}) in pipettes, were recorded from visually identified eGFP-positive tsA-201 cells ($n = 20$) in cultures transfected with plasmids encoding *SCN5A* and *eGFP*, as described in **Methods**. The bath solution was then changed sequentially to one containing 2 mM $\text{Ca}^{2+}/10$ mM Na^{+} , 2 mM $\text{Ca}^{2+}/20$ mM Na^{+} and 0 mM $\text{Ca}^{2+}/20$ mM Na^{+} and the currents were again evoked (from both HPs). The current waveforms, obtained by off-line digital subtraction of the recordings evoked from -50 mV from those evoked from -100 mV, as described in the legend to **Figure 5**, under the different ionic conditions were analyzed. In 3 of the (20) Nav1.5-expressing tsA-201 cells, inward Ca^{2+} currents were recorded (A, panel a), whereas only outward currents were observed in the other 17 cells (D, panel a). (a) Increasing the Na^{+} concentration in the bath from 0 mM (panel a; o) to 10 mM (panel b) and 20 mM (panel c; ●), increased inward current amplitudes. Exchange of the extracellular solution to one containing 0 mM Ca^{2+} (replaced by 2 mM Mg^{2+}) and 20 mM Na^{+} resulted in a further increase in the peak inward current amplitude (panel d; ■). Scale bars are 1 pA/pF and 10 ms in panel a and 10 pA/pF and 10 ms in panels b, c and d. Peak inward Ca^{2+} (o) and Na^{+} (●,■) currents for the cell in (A) are plotted in (b). The normalized voltage-dependences of activation of the currents recorded in 20 mM Na^{+} and 2 mM Ca^{2+} (●) and 20 mM Na^{+} and 0 Ca^{2+} (■) are plotted and fitted with single Boltzmanns (●: $V_{1/2} = -39$ mV, $k = 4.6$; ■: $V_{1/2} = -46$ mV, $k = 4.3$) in (c). (d) Representative outward currents recorded from an eGFP-positive, Nav1.5-expressing tsA-201 cell with 2 mM $\text{Ca}^{2+}/0$ mM Na^{+} in the bath and 145 mM K^{+} in the pipette (panel a) are shown. Increasing the Na^{+} concentration to 10 mM (panel b) and 20 mM Na^{+} in the presence (panel c) and absence of 2 mM Ca^{2+} (panel d) revealed increasing inward Na^{+} currents. Scale bars are 5 pA/pF and 10 ms in panels a, b, c and d. Peak outward K^{+} (o), and inward Na^{+} (●,■) currents for the cell in (D) are plotted as a function of the test potential in (E). The normalized voltage-dependences of activation of the peak inward currents recorded in 20 mM Na^{+} and 2 mM Ca^{2+} (●) and 20 mM Na^{+} and 0 Ca^{2+} (■) are plotted and fitted with a single Boltzmann (●: $V_{1/2} = -45$ mV, $k = 3.9$; ■: $V_{1/2} = -50$ mV, $k = 4.2$) in (f).

and LV Epi (**Figure 7(a)**, right) myocytes. The peak TTX-sensitive current densities recorded in individual cells at a test potential of -40 mV from a HP of -100 mV in LV Endo (■; $n = 16$) and LV Epi (●; $n = 10$) are presented in **Figure 7(b)**. The mean \pm SEM peak TTX-sensitive current densities in human LV Endo (■; $n = 16$) and LV Epi (●; $n = 10$)

myocytes are plotted as a function of test potential in **Figure 7(c)**.

Discussion

The experiments here identified TTX-sensitive inward Ca^{2+} currents and outward $\text{Cs}^{+}/\text{K}^{+}$ currents in myocytes isolated from adult mouse

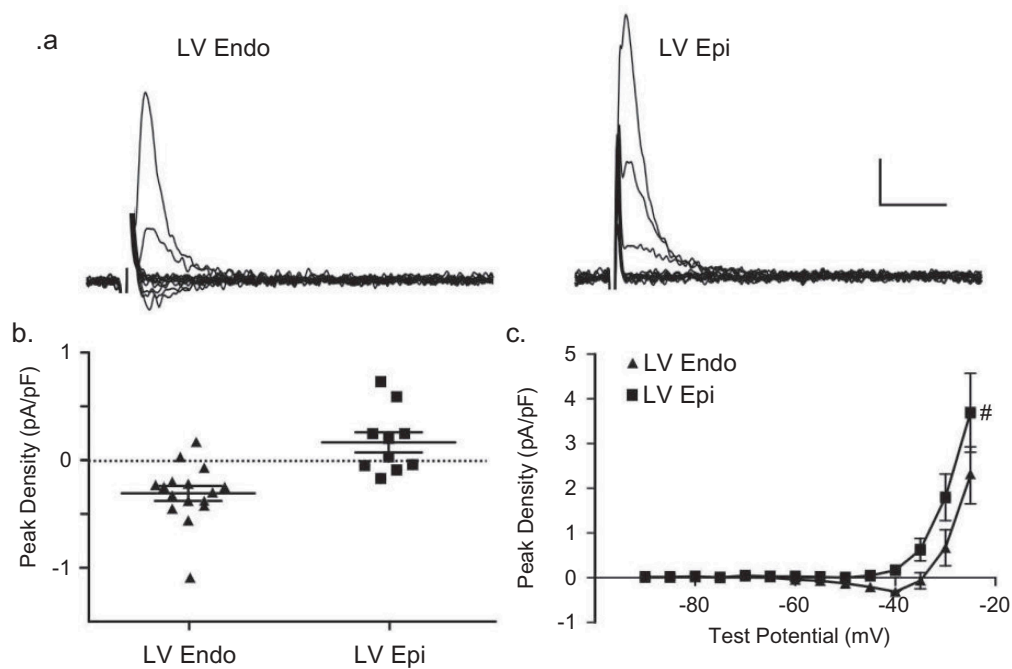


Figure 7. TTX-sensitive currents in human ventricular myocytes. With 2 mM Ca^{2+} /0 mM Na^{+} in the bath and 120 mM Cs^{+} in pipette, inward currents were measured as described in legend to Figure 2 from human LV endocardial (LV Endo) and LV epicardial (LV Epi) myocytes before and after bath applications of 10 μM TTX. (a) Representative (10 μM) TTX-sensitive current waveforms; scale bars are 0.5 pA/pF and 10 ms. (b) Peak densities of the TTX-sensitive currents evoked at -40 mV from a HP of -100 mV in human LV Endo (\bullet ; $n = 16$) and LV Epi (\blacksquare ; $n = 10$) myocytes are plotted. (c) Mean \pm SEM peak TTX-sensitive current densities in human LV Endo (\bullet ; $n = 16$) and LV Epi (\blacksquare ; $n = 10$) myocytes are plotted as a function of test potential; the densities of the currents in human LV endo and epi myocytes are significantly ($\#P < 0.05$; two-way ANOVA) different.

interventricular septum, LV apex, LV endocardial and LV endocardial myocytes, as well as in LV endocardial and epicardial myocytes isolated from non-failing human hearts, although marked differences in the relative amplitudes of the currents were observed in cells isolated from different regions of the LV in both mouse and human. The rapidly activating and inactivating, TTX-sensitive inward Ca^{2+} currents in adult mouse IVS myocytes were unaffected by Ni^{2+} and by verapamil (Figure 1) revealing that neither T-type nor L-type Ca^{2+} channels contribute. In marked contrast, the rapidly activating and inactivating inward currents and the outward $\text{Cs}^{+}/\text{K}^{+}$ currents in mouse myocytes were blocked by MTSEA, a selective inhibitor of Nav1.5-encoded channels [19,34,35].

Additional experiments revealed that TTX-sensitive inward Ca^{2+} currents and outward $\text{Cs}^{+}/\text{K}^{+}$ currents were also observed in tsA-201 cells transiently transfected with a construct encoding SCN5A (Nav1.5), and that the pharmacological and the time- and voltage-dependent properties of the heterologously expressed Nav1.5-encoded currents

were indistinguishable from those of native ventricular (TTX-sensitive inward and outward) currents in mouse and human ventricular myocytes. Also, similar to the findings in mouse ventricular myocytes, the TTX-sensitive inward Ca^{2+} and outward $\text{Cs}^{+}/\text{K}^{+}$ currents in Nav1.5-expressing tsA-201 cells were blocked by MTSEA. The simplest interpretation of these combined results is that both the inward Ca^{2+} currents and the outward $\text{Cs}^{+}/\text{K}^{+}$ currents recorded in mouse and human ventricular myocytes when extracellular Na^{+} is removed reflect currents through Nav1.5-encoded Na^{+} channels.

Regional differences in the functional expression of TTX-sensitive myocardial currents

Marked regional differences were observed in the expression of TTX-sensitive inward Ca^{2+} and outward $\text{Cs}^{+}/\text{K}^{+}$ currents in adult mouse ventricles. $I_{\text{Ca(TTX)}}$, for example, was identified in all myocytes isolated from the mouse IVS, although peak inward Ca^{2+} current amplitudes/densities were quite variable among (mouse IVS) cells. Heterogeneities in

$I_{Ca(TTX)}$ densities have also been reported in human atrial myocytes [4]. In addition, in ~40% of the mouse IVS cells studied, outward (Cs^+) currents were also observed at the more positive test potentials. Heterogeneous expression of $I_{Ca(TTX)}$ and TTX-sensitive outward (Cs^+/K^+) currents was also evident in mouse LV apex and LV free wall endocardial and epicardial myocytes, as well as in human LV endocardial and epicardial myocytes. These combined observations are quite different from the findings of Alvarez and colleagues [11] who reported no significant differences in the amplitudes/densities of $I_{Ca(TTX)}$ in different regions of infarcted rat left ventricles, suggesting species differences in the expression of TTX-sensitive currents. Alternatively, it is possible that the homogeneous expression of $I_{Ca(TTX)}$ reported by Alvarez and colleagues [11] reflects post-infarct remodeling, a hypothesis that warrants direct testing in mouse and human ventricles.

Molecular determinants of TTX-sensitive inward Ca^{2+} and outward Cs^+/K^+ currents

The sensitivity to the membrane (holding) potential and to TTX led to suggestions that $I_{Ca(TTX)}$ reflects inward Ca^{2+} flux through Nav channels encoded by the predominate Nav α subunit expressed in the heart, Nav1.5 [36]. The time- and voltage-dependent properties of $I_{Ca(TTX)}$, however, are distinct from TTX-sensitive cardiac Nav currents [1,3,4,6]. In addition, TTX-sensitive cardiac Nav currents display greater ion-selectivity and lower permeability to Cs^+ and/or K^+ [9,10]. Interestingly, it was reported that an antisense oligonucleotide directed against rat Nav1.5, although resulting in a marked reduction in I_{Na} in adult rat ventricular myocytes, had no effect on $I_{Ca(TTX)}$ [20], observations interpreted as suggesting a role(s) for novel (non Nav1.5-) Nav α subunit-encoded channels in the generation of $I_{Ca(TTX)}$ and TTX-sensitive outward Cs^+/K^+ currents.

The experiments here, however, revealed TTX-sensitive inward Ca^{2+} currents and outward Cs^+/K^+ currents in tsA-201 cells transiently transfected with a cDNA construct encoding human SCN5A (Nav1.5). Similar to the observations in mouse and human ventricular myocytes, these experiments also revealed TTX-sensitive inward Ca^{2+} currents

in a subset of the transiently transfected tsA-201 cells and outward Cs^+/K^+ currents in the others. The observed regional differences in the functional expression of TTX-sensitive inward Ca^{2+} currents and outward Cs^+/K^+ currents in mouse and human ventricular myocytes suggest that native Nav1.5-encoded cardiac Na^+ channels are molecularly heterogeneous. Interestingly, it was recently reported that there are marked differences in *Scn5a* transcript expression levels and functional Nav current densities in adult mouse left and right ventricular endocardium and epicardium [37]. Cell type-specific differences in the densities/properties of TTX-sensitive, cardiac Nav1.5-encoded currents could also reflect the functional consequences of the differential splicing of *Scn5a/SCN5A* transcripts [38], as has been demonstrated for invertebrate Na^+ and Ca^{2+} channels [39–41], as well as for the critical tight junction protein, claudin-10 [42,43] and TRPM3 [44]. Regional differences in the expression/functioning of Nav channel accessory subunits [45] and/or of other Nav channel regulatory proteins [46,47], as well as heterogeneities in post-translational modifications of Nav1.5 [48] and/or of one or more Nav channel accessory/regulatory proteins [45–47], could also play a role. Additional experiments are needed to define the molecular mechanisms underlying the observed regional differences in the functional expression and properties of native Nav1.5-encoded cardiac Na^+ channels in mouse and human ventricles.

Functional implications of heterogeneous expression of TTX-sensitive myocardial currents

The observed regional differences in the functional expression of TTX-sensitive inward Ca^{2+} currents and outward Cs^+/K^+ currents suggest that there are (at least) two molecularly distinct types of *Scn5a/SCN5A*-encoded channels in both mouse and human LV myocytes. The molecular determinants of these channels may also be distinct from the Nav1.5-encoded channels that mediate inward Na^+ flux and control cardiac myocyte action potential generation and propagation that display low Ca^{2+} and Cs^+/K^+ permeability [13,14]. Together with the observation that $I_{Ca(TTX)}$ activates at potentials negative to the activation of I_{Na} , these results suggest

a possible role for Ca^{2+} entry through $I_{\text{Ca(TTX)}}$ channels in regulating myocardial excitability and rhythmicity, particularly in the subthreshold range of membrane potentials. If there are changes in the relative expression and/or the distribution of $I_{\text{Ca(TTX)}}$ channels under pathophysiological conditions [11], these could have functional consequences, perhaps contributing to the generation and maintenance of cardiac arrhythmias. Studies focused on defining the molecular basis of functional myocardial Nav1.5-encoded channel diversity and the mechanisms controlling the functional expression of these channels will be needed to explore these hypotheses directly.

Competing interests

The authors have no competing financial interests to declare.

Disclosure statement

No potential conflict of interest was reported by the authors.

Funding

This work was supported by the National Heart, Lung, and Blood Institute Grant (R01 HL-034161 to JMN) and by a Washington University School of Medicine intramural research grant (to CWB); National Institutes of Health [HL-034161];

Author contributions

WW, RLM, JMN and CWB contributed to the conception of the work and the design of the experiments. WW conducted the electrophysiological experiments and RLM executed the cell transfections. WW and JMN analyzed the acquired electrophysiological data. WW, JMN and CWB contributed to the interpretation of the data and the writing of the manuscript.

All authors approved the final version of the manuscript submitted for publication and all agree to be accountable for all aspects of the work presented.

References

- [1] Meves H, Vogel W. Calcium inward currents in internally perfused giant axons. *J Physiol Lond.* 1973;235:225–265.
- [2] Benoit E, Corbier A, Dubois JM. Evidence for two transient sodium currents in the frog node of Ranvier. *J Physiol Lond.* 1985;361:339–360.
- [3] Akaike N, Takahashi K. Tetrodotoxin-sensitive calcium-conducting channels in the rat hippocampal CA1 region. *J Physiol Lond.* 1992;450:529–546.
- [4] Lemaire S, Piot C, Seguin J, et al. Tetrodotoxin-sensitive Ca^{2+} and Ba^{2+} currents in human atrial cells. *Recept Channels.* 1995;3:71–81.
- [5] Cole W, Chartier CD, Martin M, et al. Ca^{2+} permeation through Na^{+} channels in guinea pig ventricular myocytes. *Am J Physiol Heart Circ.* 1997;273:H128–H137.
- [6] Aggarwal R, Shorofsky SR, Goldman L, et al. Tetrodotoxin-blockable calcium currents in rat ventricular myocytes; a third type of cardiac cell sodium current. *J Physiol Lond.* 1997;505:353–369.
- [7] Santana LF, Gómez AM, Lederer WJ. Ca^{2+} flux through promiscuous cardiac Na^{+} channels: slip-mode conductance. *Science.* 1998;279:1027–1033.
- [8] Heubach JF, Köhler A, Wettwer E, et al. T-Type and tetrodotoxin-sensitive Ca^{2+} currents coexist in guinea pig ventricular myocytes and are both blocked by mibefradil. *Circ Res.* 2000;86:628–635.
- [9] Chen-Izu Y, Sha Q, Shorofsky SR, et al. $I_{\text{Ca(TTX)}}$ channels are distinct from those generating the classical cardiac Na^{+} current. *Biophys J.* 2001;81:2647–2659.
- [10] Guatimosim S, Sobie EA, Dos Santos CJ, et al. Molecular identification of a TTX-sensitive Ca^{2+} current. *Am J Physiol Cell Physiol.* 2001;280:C1327–1339.
- [11] Alvarez JL, Salinas-Stefanon E, Orta G, et al. Occurrence of a tetrodotoxin-sensitive calcium current in rat ventricular myocytes after long-term myocardial infarction. *Cardiovasc Res.* 2004;63:653–661.
- [12] Bodi I, Mikala G, Koch SE, et al. The L-type calcium channel in the heart: the beat goes on. *J Clin Invest.* 2005;115:3306–3317.
- [13] Nerbonne JM, Kass RS. Molecular physiology of cardiac repolarization. *Physiol Rev.* 2005;85:1205–1253.
- [14] Priest BT, McDermott JS. Cardiac ion channels. *Channels.* 2015;9:352–359.
- [15] Lei M, Jones SA, Liu J, et al. Requirement of neuronal- and cardiac-type sodium channels for murine sinoatrial node pacemaking. *J Physiol Lond.* 2004;559:835–848.
- [16] Kaufmann SG, Westenbroek RE, Zechner C, et al. Functional protein expression of multiple sodium channel alpha- and beta-subunit isoforms in neonatal cardiomyocytes. *J Mol Cell Cardiol.* 2010;48:261–269.
- [17] Kaufmann SG, Westenbroek RE, Maass AH, et al. Distribution and function of sodium channel subtypes in human atrial myocardium. *J Mol Cell Cardiol.* 2013;61:133–141.
- [18] Westenbroek RE, Bischoff S, Fu Y, et al. Localization of sodium channel subtypes in mouse ventricular myocytes using quantitative immunocytochemistry. *J Mol Cell Cardiol.* 2013;64:69–78.
- [19] Mishra S, Reznikov V, Maltsev VA, et al. Contribution of sodium channel neuronal isoform Nav1.1 to late sodium current in ventricular myocytes from failing hearts. *J Physiol Lond.* 2015;593:1409–1427.

- [20] Sha Q, Robinson SW, McCulle SL, et al. An antisense oligonucleotide against H1 inhibits the classical sodium current but not $I_{Ca(TTX)}$ in rat ventricular cells. *J Physiol Lond.* **2003**;547:435–440.
- [21] Su Z, Sheets M, Ishida H, et al. Saxitoxin blocks L-type I_{Ca} . *J Pharmacol Exp Ther.* **2004**;308:324–329.
- [22] Hegyi B, Bárándi L, Komáromi I, et al. Tetrodotoxin blocks L-type Ca^{2+} channels in canine ventricular cardiomyocytes. *Pflügers Arch.* **2012**;464:167–174.
- [23] Bodi I, Nakayama H, Schwartz A. Tetrodotoxin-sensitive Ca^{2+} currents, but no T-type currents in normal, hypertrophied, and failing mouse cardiomyocytes. *J Cardiovasc Pharmacol.* **2016**;68:452–464.
- [24] Sun H, Varela D, Chartier D, et al. Differential interactions of Na^+ channel toxins with T-type Ca^{2+} channels. *J Gen Physiol.* **2008**;132:101–113.
- [25] Xu H, Guo W, Nerbonne JM. Four kinetically distinct depolarization-activated K^+ currents in adult mouse ventricular myocytes. *J Gen Physiol.* **1999**;113:661–678.
- [26] Brunet S, Aimond F, Li H, et al. Heterogeneous expression of repolarizing voltage-gated K^+ currents in adult mouse ventricles. *J Physiol Lond.* **2004**;559:103–120.
- [27] Haim TE, Wang W, Flagg TP, et al. Palmitate attenuates myocardial contractility through augmentation of repolarizing K_v currents. *J Mol Cell Cardiol.* **2010**;48:395–405.
- [28] Osterrieder W, Yang QF, Trautwein W. Conductance of the slow inward channel in the rabbit sinoatrial node. *Pflügers Arch.* **1982**;394:85–89.
- [29] Bean BP. Two kinds of calcium channels in canine atrial cells. Differences in kinetics, selectivity and pharmacology. *J Gen Physiol.* **1985**;86:1–30.
- [30] Bonvallet R, Rougier O. Existence of two calcium currents recorded at normal calcium concentrations in single frog atrial cells. *Cell Calcium.* **1989**;10:499–508.
- [31] Nargeot J. A tale of two (calcium) channels. *Circ Res.* **2000**;86:613–615.
- [32] Perez-Reyes E. Molecular physiology of low-voltage-activated T-type calcium channels. *Physiol Rev.* **2003**;83:117–161.
- [33] Tytgat J, Vereecke J, Carmeliet E. Differential effects of verapamil and flunarizine on cardiac L-type and T-type Ca channels. *Naunyn Schmiedebergs Arch Pharmacol.* **1988**;337:690–692.
- [34] Biet M, Barajas-Martínez H, Ton AT, et al. About half of the late sodium current in cardiac myocytes from dog ventricle is due to non-cardiac-type Na^+ channels. *J Mol Cell Cardiol.* **2012**;53:593–598.
- [35] Haufe V, Cordeiro JM, Zimmer T, et al. Contribution of neuronal sodium channels to the cardiac fast sodium current I_{Na} is greater in dog heart Purkinje fibers than ventricles. *Cardiovasc Res.* **2005**;65:117–127.
- [36] Zimmer T, Haufe V, Blechschmidt S. Voltage-gated sodium channels in the mammalian heart. *Glob Cardiol Sci Pract.* **2014**;4:449–463.
- [37] Veerman CC, Podliesna S, Tadros R, et al. The Brugada syndrome susceptibility gene *HEY2* modulates cardiac transmural ion channel patterning and electrical heterogeneity. *Circ Res.* **2017**;121:537–548.
- [38] Schroeter A, Walzik S, Blechschmidt S, et al. Structure and function of splice variants of the cardiac voltage-gated sodium channel Nav1.5. *J Mol Cell Cardiol.* **2010**;49:16–24.
- [39] Zhang T, Liu Z, Song W, et al. Molecular characterization and functional expression of the DSC1 channel. *Insect Biochem Mol Biol.* **2011**;41:451–458.
- [40] Senatore A, Monteil A, van Minnen J, et al. NALCN ion channels have alternative selectivity filters resembling calcium channels or sodium channels. *PLoS One.* **2013**;8:e55088.
- [41] Stephens RF, Guan W, Zhorov BS, et al. Selectivity filters and cysteine-rich extracellular loops in voltage-gated sodium, calcium, and NALCN channels. *Front Physiol.* **2015**;6:153.
- [42] Van Itallie CM, Rogan S, Yu A, et al. Two splice variants of claudin-10 in the kidney create paracellular pores with different ion selectivities. *Am J Physiol Renal Physiol.* **2006**;291:F1288–F1299.
- [43] Günzel D, Stuiver M, Kausalya PJ, et al. Claudin-10 exists in six alternatively spliced isoforms that exhibit distinct localization and function. *J Cell Sci.* **2009**;122:1507–1517.
- [44] Oberwinkler J, Philipp SE. TRPM3. *Handb Exp Pharmacol.* **2007**;179:253–267.
- [45] Abriel H. Cardiac sodium channel Nav1.5 and interacting proteins: physiology and pathophysiology. *J Mol Cell Cardiol.* **2010**;48:2–11.
- [46] Petitprez S, Zmoos AF, Oгородnik J, et al. SAP97 and dystrophin macromolecular complexes determine two pools of cardiac sodium channels Nav1.5 in cardiomyocytes. *Circ Res.* **2011**;108:294–304.
- [47] Eichel CA, Beuriot A, Chevalier MY, et al. Lateral membrane-specific MAGUK CASK down-regulates Nav1.5 channel in cardiac myocytes. *Circ Res.* **2016**;119:544–556.
- [48] Marionneau C, Abriel H. Regulation of the cardiac Na^+ channel Nav1.5 by post-translational modifications. *J Mol Cell Cardiol.* **2015**;82:36–47.